Measurement and modeling of HF channel directional spread characteristics for northerly paths

E. M. Warrington,[1] A. J. Stocker,[1] and D. R. Siddle[1]

[1]   The northerly ionosphere is a dynamic propagation medium that causes HF signals reflected from this region to exhibit delay spreads and Doppler shifts and spreads that significantly exceed those observed over midlatitude paths. Since the ionosphere is not perfectly horizontally stratified, the signals associated with each propagation mode may arrive at the receiver over a range of angles in both azimuth and elevation. Such large directional spreads may have a severe impact on radio systems employing multielement antenna arrays and associated signal-processing techniques since the signal environment does not comprise a small number of specular components as often assumed by the processing algorithms. In order to better understand the directional characteristics of HF signals reflected from the northerly ionosphere, prolonged measurements have recently been made over two paths: (1) from Svalbard to Kiruna, Sweden, and (2) from Kirkenes, Norway, to Kiruna. An analysis of these data is presented in this paper. The directional characteristics are summarized, and consideration is given to modeling the propagation effects in the form of a channel simulator suitable for the testing of new equipment and processing algorithms.

1.   Introduction

[2]   The northerly ionosphere is a dynamic propagation medium that causes HF signals reflected from this region to exhibit delay spreads and Doppler shifts and spreads that significantly exceed those observed over midlatitude paths [see, e.g., *Angling et al.*, 1998]. These Doppler effects are due to large-scale motion of the ionosphere and/or the turbulent motion of plasma irregularities that are a common feature of the auroral and polar cap ionospheres. From the perspective of communications systems, such large delay and Doppler spreads can result in a significant degradation in system performance (e.g., in achievable data throughput). Discussion of this aspect is given by *Angling et al.* [1998] and *Jodalen et al.* [2001] who report the results from an extensive measurement campaign over a number of high-latitude paths using the DAMSON system and relate their results to anticipated modem performance.

[3]   Since the ionosphere is not perfectly horizontally stratified, the signals associated with each propagation

mode may arrive at the receiver over a range of angles in both azimuth and elevation. *Warrington* [1998] reported preliminary measurements of the directional characteristics of signals radiated from the sounder system (DAMSON) described by *Angling et al.* [1998], and noted that considerable variation in the direction of arrival of the various signal components was often evident. Such large directional spreads may have a severe impact on n channel radio systems (e.g., adaptive beamformers and direction finders) since the signal environment does not comprise a small number of specular components as often assumed by the processing algorithms. The effect of directional spread on superresolution HF-DF systems has been presented by *Jenkins* [1994] and by *Warrington et al.* [2000b], and a direction finding algorithm (SPIRE) designed specifically to operate with spatially diffuse signals has been developed by *Read* [1999]. *Warrington et al.* [2000a] reported the possibility of employing spatial filtering to reduce apparent delay and Doppler spreads. Simulations of propagation at northerly latitudes that include directional spreading have been presented by *Zaalov et al.* [2003, 2005].

[4]   Channel simulation is frequently employed in system development, most often (perhaps) to determine the effect of various propagation conditions on modem performance in systems employing a single receiver channel.

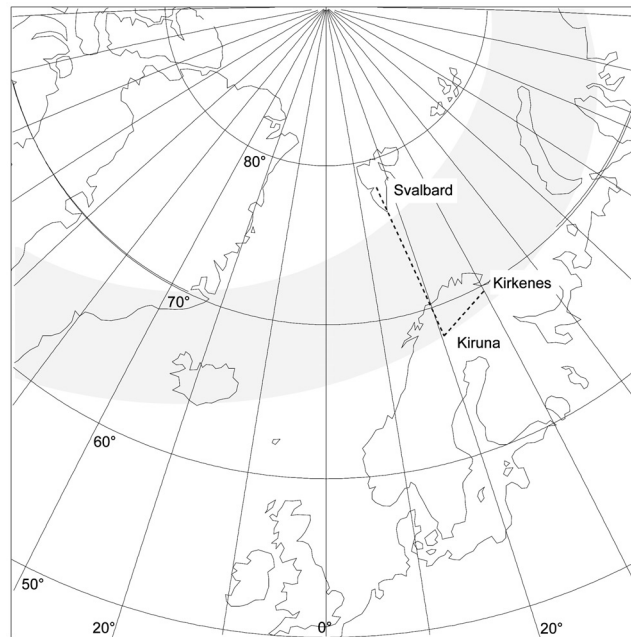[1]Department of Engineering, University of Leicester, Leicester, UK.

Figure 1. Map showing the Svalbard-Kiruna and Kirkenes-Kiruna paths.

A popular foundation for such channel simulators (see, for example, International Telecommunication Union recommendation ITU-R F.1487 [*International Telecommunication Union*, 2000]) is the model presented by *Watterson et al.* [1970] on the basis of measurements made over midlatitude paths. The ITU-R recommendation F.1487 includes a methodology for quantitative testing of HF modems together with a range of channel parameters that are appropriate for low-latitude, midlatitude, and high-latitude paths. Models have also been developed with a physical basis appropriate to a wide range of ionospheric conditions [*Gherm et al.*, 2005], however these have yet to be incorporated in simulators used for hardware testing (this is, presumably, the next stage in development) and are not applicable to cases with strong scintillation such as occurs over high-latitude paths. Current simulators aimed at single receiver channels have limited application when n channel receiver systems are employed (e.g., adaptive spatial filtering systems or direction finding systems) for which the directional characteristics, in addition to delay and Doppler effects, are of crucial importance. This paper is concerned with measurements of the directional spread characteristics of HF signals received over northerly paths and with developments toward a channel simulator incorporating such directional effects.

2. Measurements of Spatial Effects

[5] The measurements considered in this paper were made over two paths to Kiruna in northern Sweden.

Transmitters operating on six frequencies between 4 and 20 MHz were located at Adventdalen on Svalbard (giving a path length of 1152 km and a bearing at the receiver of 355°) and at Bjørnsund near to Kirkenes in northern Norway (430 km, bearing 61°) (see Figure 1).

[6] The radiated signals comprised 2 s sequences of 13-bit Barker coded PSK pulses modulated at (usually) 2000 baud with a repetition rate of 66.7 coded pulses per second. Since the transmitter and receiver systems were synchronized to GPS, the absolute time of flight of the signals may be determined. The signals were received with a large sampled aperture antenna array, each element of which was connected to a separate receiver. The complex amplitudes of the signals received on each antenna within the array were sampled simultaneously 10000 times per second and the data processed to provide a measure of the relative times of flight of the propagating modes and their associated Doppler spectra (see the method employed by the DAMSON system, described by *Davies and Cannon* [1993]). In this way, the signal was split into components distinguished by time of flight, Doppler frequency and by antenna position in the receiving array. A direction finding algorithm (usually a modified version of the Capon algorithm [*Featherstone et al.*, 1997]) was then applied to each signal component in turn in order to estimate the directional characteristics of the received signal. Although the modified Capon algorithm was usually employed in the processing of the experimental data, the choice of algorithm is not particularly critical (see *Warrington et*

al. [2000b] for a discussion of the behavior of various algorithms in the presence of diffuse signal energy). Note that when several signal components closely separated in direction of arrival are present in a single delay-Doppler cell, the DF algorithm may produce a single estimate of the direction of arrival. This arises from the limited resolving capability of the DF algorithm and it is expected that the estimated direction of arrival will usually be bounded by the limits of the direction of arrival spread within the cell. The precise value of the estimated direction of arrival will vary with time as the relative phases and amplitudes of the constituent components within the delay-Doppler cell change.

[7] An example measurement taken over the Kirkenes-Kiruna path on 30 March 2004 is presented in Figure 2. On the delay-Doppler plot, the sidelobes of the pulse compression along the time axis have been suppressed (the despread pulse from a Barker-13 coded sounding pulse has sidelobes at best approximately -22 dB relative to the peak). The measured elevation angles of arrival and the time of flight indicate that propagation was probably by a 1F mode. Note, however, that owing to the limited aperture of the antenna array, comparatively poor accuracy was achieved in the elevation angle measurements. For this reason, azimuthal measurements are considered here in most detail. It should also be noted that differences in the reference frequencies at the transmitter and receiver sites gives rise to a frequency offset of the received signals of approximately -5 Hz in this instance (the offset due to the reference differences cannot be determined by examination of a single measurement and is established by examination of measurements obtained at this frequency over a period of several days). Ionospheric variations then tend to cause Doppler shifts and spreads of a few hertz from this offset frequency.

[8] A marked relationship is evident between the Doppler frequency and the measured bearing (see middle frame). Signal components arriving at the receiver from directions with higher bearing angles than the great circle direction have positive Doppler shifts imposed, whereas signals arriving from directions with lower bearing angles than the great circle direction have negative Doppler shifts imposed (in this instance, the relationship between the bearing and the Doppler frequency is approximately 5 degrees/Hz). This observation is consistent with reflections/scattering from irregularities in the ionospheric electron density distribution drifting with the convection flow. At this time, the SuperDARN radars observed an east-west convection flow with velocities of several hundred meters per second at latitudes similar to the Kirkenes-Kiruna path. For irregularities drifting in a westerly direction, positive Doppler shifts would be imposed on any signal components scattered from irregularities to the east of the great circle direction where the motion of the scatterers was in a direction tending to

shorten the path and negative Doppler shifts imposed on those scattered components to the west of the great circle path direction where the motion of the scatterers was in a direction tending to lengthen the path.

[9] Agreement between the broad characteristics of the convection flows deduced from SuperDARN and the sense of any directionally dependent Doppler effects was frequently obtained. However, extensive comparisons of the radar measurements with the received sounding signals did not yield further useful results. In particular, there was not a one-to-one agreement between the magnitude of the observed Doppler effects and the flow velocities estimated by SuperDARN.

[10] A second example is presented in Figure 3. In this case, the signal comprises two modes (1E and 1F) which are not fully resolved in time of flight. Of particular note is the large range of azimuth angles present, ranging from just over $80°$ to around $30°$, a spread of some $50°$ (the spread of azimuths containing 80% of the power is $41°$).

3. Overall Spread Measurements

[11] The characteristics of the received signal can vary considerably (see, for example, Figures 2 and 3) and consequently it is not easy to make general statements about the signal structure, other than at times it can be very complex. One way of summarizing the data is in terms of the overall power spread in azimuth and elevation. In order to achieve this, observations of the form given in Figures 2 and 3 have been processed as follows. First, the power received was found as a function of azimuth and elevation by taking the azimuth and elevation values of each pixel in the scattering function plots and summing the power on an azimuth-elevation grid with $1°$ resolution (top plot of Figure 4). The resulting power values are then summed for each azimuth to produce the middle plot of Figure 4, and similarly for elevation (bottom plot of Figure 4). After determining a threshold value on the basis of the noise floor (at a level higher than -15dB relative the peak power; the horizontal line marked on the middle and bottom plots in Figure 4), the spread is calculated as the minimum range of azimuths or elevations that contain 80% of the power.

[12] In order to determine the probability of occurrence of various values of azimuth and elevation spread, the cumulative distribution functions for all observations on a monthly basis have been calculated. Only cases with a strong signal (peak to mean power ratio > 3.5, corresponding to an SNR of approximately -5dB) that were free from interferers have been included in the statistical analysis. Median, upper quartile, upper decile and 95% level spread values for a number of months and two frequencies are given in Tables 1 and 2. There is little variation in the median for either frequency being
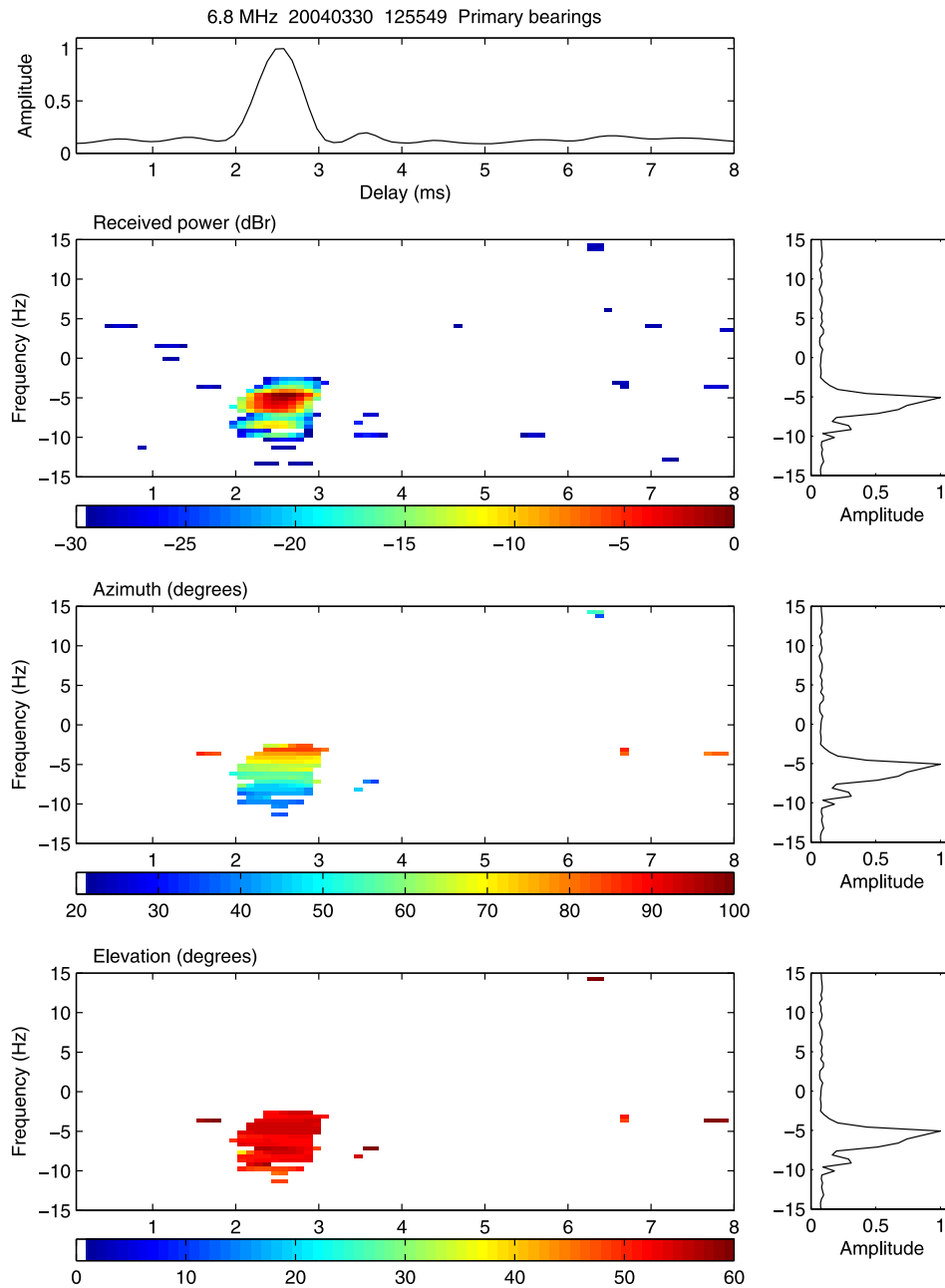
Figure 2. Example sounding for the Kirkenes-Kiruna path at 6.8 MHz on 30 March 2004 at 1255 UT. The top plot shows the signal amplitude as a function of time of flight (TOF). The three main plots display the received power (normalized such that 0 dBr refers to the peak power), azimuth (in the range 20°–100°; great circle path is 61°), and elevation (in the range 0°–60°) as a function of Doppler frequency and TOF. The right-hand plots show the signal amplitude as a function of Doppler frequency (note that these three frames are identical).
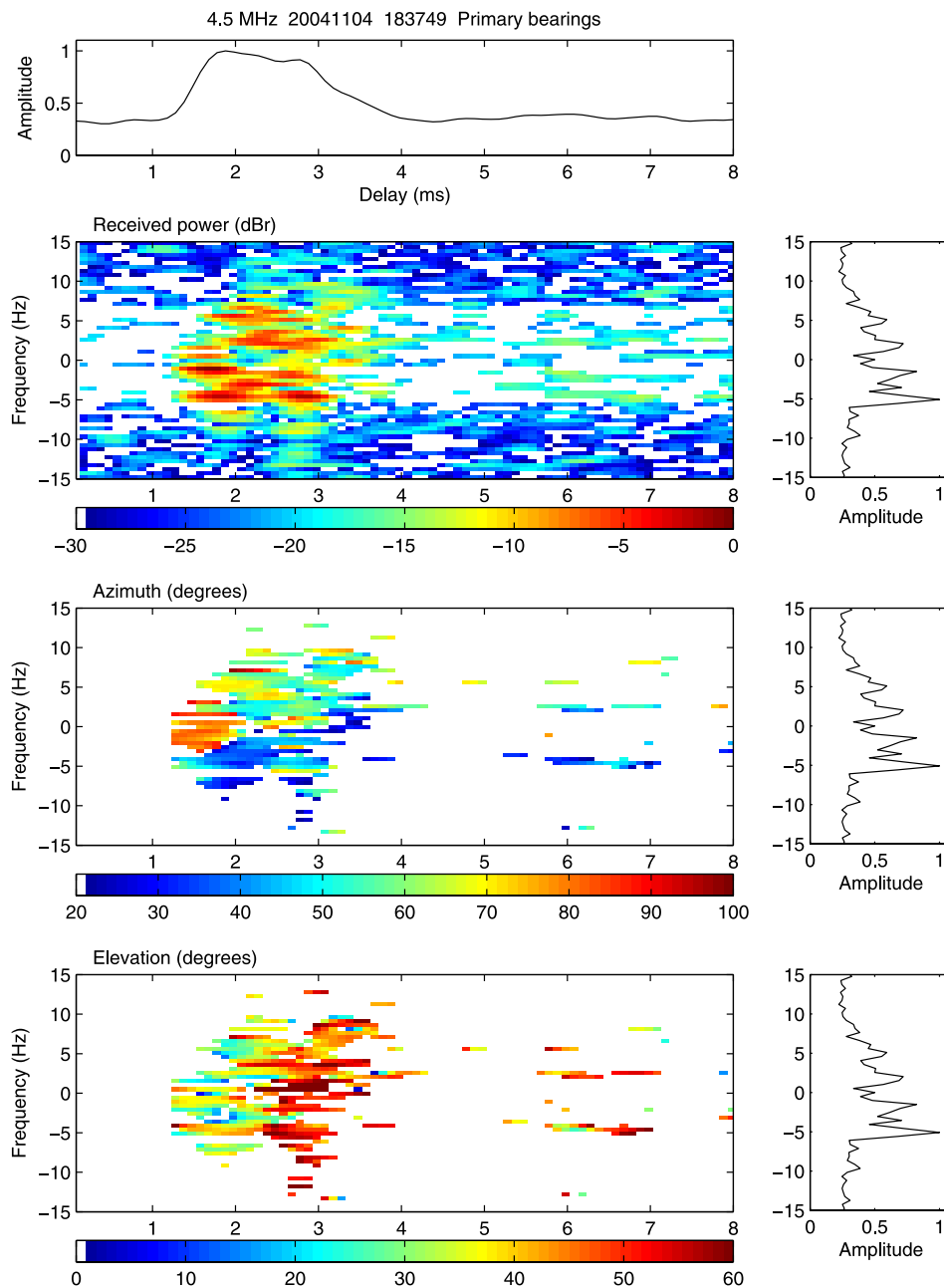
Figure 3. As for Figure 2 but for 4.455 MHz on 4 November 2004, 1837 UT.

3° for 4.455 MHz and 2–3° for 6.78 MHz. The 95% values show considerable variation, with no clear seasonal variation, although the lowest values are found in the summer months. The high value of azimuth spread at 4.455 MHz in August 2004, appears to be a result of a number of instances of simultaneous propagation via 1E and 1F modes where the direction of arrival for each of the modes is different as well as cases similar to that presented in Figures 3 and 4. The high value of azimuth spread in July 2004 for 6.78 MHz arises from nine very spread cases that occurred on one day (25 July), and the relatively low number of observations in that month. If that day is removed from the calculations, the spread at the 95% level is 4°.

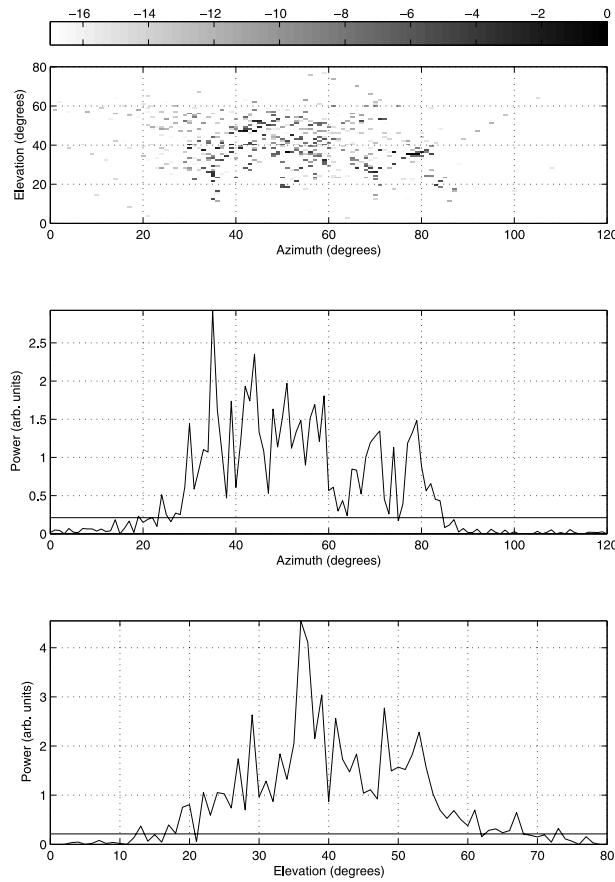**Figure 4.** Signal at 4.455 MHz transmitted at Kirkenes and received at Kiruna, 4 November 2004, at 1837 UT: (top) power received as a function of azimuth and elevation, (middle) power as a function of azimuth, and (bottom) power as a function of elevation. The azimuth spread is 41°, and the elevation spread is 26°.

[13] The azimuth, composite and effective multipath, and Doppler spreads at the 95% occurrence level for both paths and for the years 2003, 2004, and 2005 (up to 17 June) are given in Table 3. The multipath and Doppler spread parameters are defined here in a similar manner to that employed by *Angling et al.* [1998]. The composite multipath spread is a measure of the overall temporal spread of the incoming signal, however no account is taken of the relative powers contained within the various detected modes. Consequently, measurements have also been included of a parameter, known as the effective multipath spread, which takes the relative modal powers into account and was found to provide better results than the composite multipath spread when employed in modem tests using an HF channel simulator [*Angling*

and Davies, 1999]. The definition of the three spread parameters is as follows.

3.1. Composite Multipath Spread

[14] This parameter is taken as the temporal separation between the rising edge of the first detected mode and the falling edge of the last detected mode, with a correction applied for the width of the transmitted pulse.

3.2. Effective Multipath Spread

[15] This is a measure of multipath spread which gives a good agreement between the expected modem characteristics and the modem performance under the complex propagation conditions encountered at high latitudes [*Angling and Davies*, 1999]. The equivalent multipath spread is calculated for a pair of modes by determining the multipath separation between the rising edge of the central 80% power region of the first (in delay time) mode and the trailing edge of the central 80% power region of the last mode (corrected for the transmitted pulse width) and weighting the separation with the ratio of the two modes' total powers. This ratio is always arranged so as to be equal or less than unity. This procedure is applied to each pair of modes in turn and the equivalent multipath spread taken as the maximum value found. If only a single mode is present, then the effective multipath spread is taken to be the mode's 80% power spread, again corrected for the width of the transmitted pulse.

Table 1. Median, Upper Quartile, Upper Decile, and 95% Values of Azimuth Spread for the Kirkenes-Kiruna Path at 4.455 MHz[a]

	Cases	50%	75%	90%	95%
March 2004	373	3	6	11	20
April 2004	671	3	6	12	18
May 2004	652	3	6	13	22
June 2004	815	3	4	8	13
July 2004	349	3	6	13	18
Aug 2004	512	3	7	17	28
Sept 2004	744	3	6	14	22
Oct 2004	947	3	6	17	25
Nov 2004	292	3	7	15	22
Dec 2004	3075	3	6	13	22
Jan 2005	2335	3	6	13	22
Feb 2005	4285	3	6	14	22
March 2005	4659	3	5	11	18
April 2005	4795	3	7	17	27
May 2005	2173	3	6	13	20

[a]Values of azimuth spread are in degrees. Note that the transmission schedule changed in December 2004, hence the marked increase in the number of cases.

Table 2. Median, Upper Quartile, Upper Decile, and 95% Values of Azimuth Spread for the Kirkenes-Kiruna Path at 6.780 MHz[a]

	Cases	50%	75%	90%	95%
March 2004	260	2	4	7	12
April 2004	475	2	5	12	19
May 2004	257	2	3	6	11
June 2004	604	2	3	5	8
July 2004	56	2	7	15	21
Aug 2004	126	2	3	5	8
Sept 2004	211	2	4	9	14
Oct 2004	401	2	4	9	15
Nov 2004	190	3	5	12	17
Dec 2004	1265	3	5	10	16
Jan 2005	1332	3	5	12	21
Feb 2005	2575	3	6	15	24
March 2005	2016	3	5	9	17
April 2005	1410	3	6	13	20
May 2005	911	2	5	13	25

[a]Values of azimuth spread are in degrees. Note that the transmission schedule changed in December 2004, hence the marked increase in the number of cases.

3.3. Composite Doppler Spread

[16] This parameter is defined as the narrowest spectral width containing 80% of the received signal power. In all cases, a correction is applied for the base noise level.

[17] While the data coverage is generally good, it should be noted that in 2003 data were only collected on the Svalbard-Kiruna path for July. This period covers the declining phase of the sunspot cycle with the smoothed sunspot number falling from 80 in January 2003 to 30 at the beginning of 2005. For the shorter path, the azimuth spread tends to increase slightly with increasing frequency (most apparent in 2003) probably because the higher frequencies are more likely to be closer to the MUF and the direction of arrival more sensitive to small variations in the electron density. For the longer path, the opposite is the case with the azimuth spread tending to decrease with increasing frequency. This is likely to result from the higher frequencies being more likely to propagate via a single hop and, particularly at night, to propagate via an *E* region (auroral or sporadic) mode for which the azimuth spread is generally low. It is also interesting to note that the observed Doppler spread tends to increase with increasing azimuth spread (Figure 5), although the exact relationship depends on both the frequency and the path. This result is consistent with a study of a selection of the individual cases, where a larger range of azimuths is often found with modes that are also spread in Doppler.

[18] The composite multipath and Doppler spreads in Table 3 can be compared with the results presented by *Angling et al.* [1998] for observations they made over

similar paths in 1995 (close to sunspot minimum with sunspot numbers ~15–25). For the Svalbard to Kiruna path, the composite multipath spread tends to decrease with frequency in Angling et al.'s observations, since propagation will tend to be via fewer hops at the higher frequencies, whereas the values do not seem to depend on frequency in the measurements presented

Table 3. Values of Azimuth, Composite and Effective Multipath Spreads, and Doppler Spread at the 95% Level for Peak-to-Mean Power Ratios Greater Than 3.5[a]

	Svalbard-Kiruna			Kirkenes-Kiruna		
Frequency, MHz	2003	2004	2005	2003	2004	2005
Azimuth Spread, deg						
4.5	4	18	16	16	21	22
5.8	12	15	–	18	12	–
6.8	9	12	11	18	15	21
9.0	6	9	4	19	11	12
9.9	4	6	–	21	–	–
11.2	5	7	–	25	21	–
14.4	5	4	–	–	–	–
20.0	3	–	–	–	–	–
Composite Multipath Spread, ms						
4.5	7.7	6.9	5.1	4.6	5.2	5.0
5.8	12.0	7.3	–	4.6	6.1	–
6.8	11.6	5.3	4.9	4.2	4.4	4.8
9.0	5.0	10.2	8.1	4.6	4.2	6.2
9.9	12.3	9.6	–	13.0	–	–
11.2	11.7	5.8	–	7.3	5.9	–
14.4	11.5	3.8	–	6.7	5.5	–
20.0	1.2	–	–	–	5.3	–
Effective Multipath Spread, ms						
4.5	0.3	1.7	0.5	0.7	0.5	0.6
5.8	1.5	1.2	–	0.9	0.6	–
6.8	1	0.8	0.6	0.6	0.3	0.3
9.0	0.5	0.8	0.3	0.5	0.2	0.2
9.9	0.4	0.2	–	0.6	–	–
11.2	0.2	0.2	–	0.9	0.3	–
14.4	0.1	0.1	–	1.0	0.8	–
20.0	0.1	–	–	–	0.4	–
Composite Doppler Spread, Hz						
4.5	1	3.1	2.6	1.5	1.5	2
5.8	2	3.5	–	2	1.1	–
6.8	2	2.5	2.5	2.5	2.6	3.7
9.0	2	3.6	1.5	6.4	5.8	9.4
9.9	2	1.6	–	8.1	–	–
11.2	2	2.5	–	13.8	12.4	–
14.4	2.5	3.6	–	29.8	28.2	–
20.0	1.5	–	–	–	39.2	–

[a]Observations in 2005 were made at 4.5 and 6.8 MHz until 17 June and at 9.0 MHz from 15 April until 17 June. In 2003, observations on the Svalbard path were only made during July. Observations at 9.9 MHz transmitted from Kirkenes were made to the end of March 2003. Azimuth spread observations at 14.4 and 20.0 MHz on the Kirkenes path were contaminated by array sidelobes. Cases with fewer than 50 points are omitted.
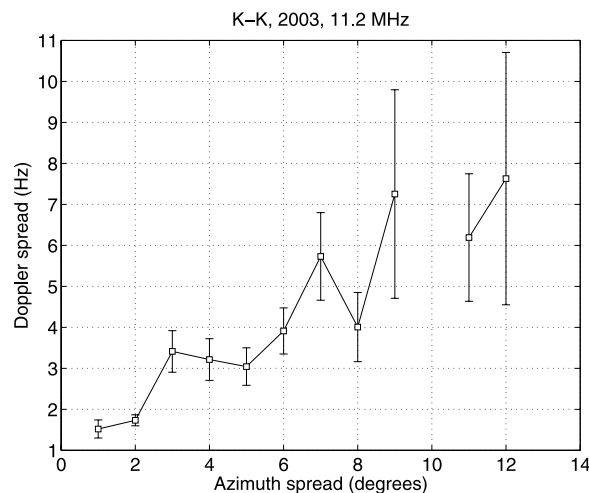
Figure 5. Doppler spread versus azimuth spread for Kirkenes-Kiruna, 11.2 MHz, 2003.

here. Furthermore, the magnitude of the spread is also different; the recent measurements having spreads that are much larger, particularly at the higher frequencies. Composite multipath spread values derived from VOACAP and ICEPAC predictions using method 25 ("All modes table") cannot explain the spreads larger than a few ms seen in either set of measurements. However, these models are limited to on−great circle propagation via ionospheric reflection and therefore do not include other propagation mechanisms (e.g., scatter) that might be present in the observations. In the case of the shorter paths (Harstad-Kiruna in 1995, and Kirkenes-Kiruna in 2003–2005), the trend in 2003 is similar to that in the earlier observations; smaller multipath spreads being found at low frequencies (4.5–9.0 MHz) and larger ones at middle frequencies (9.9–14.4 MHz). Although the trend in 2004 and 2005 is not so clear, the composite multipath spread in the new data is similar in magnitude to that in the older data except at the middle frequencies where the recent data shows smaller spreads. *Angling et al.* [1998] suggested that the large multipath spreads arose as a result of the signal being reflected from the auroral zone well to the north of the propagation path. That this auroral propagation mechanism appears to occurs less frequently on the Kirkenes-Kiruna path may result from the different geometry (Kirkenes-Kiruna is aligned more north-south than the Harstad-Kiruna path) and length or perhaps because the measurements were taken at a different phase of the solar cycle. It is also noteworthy that the current observations generally cover a broader range of seasons than the earlier observations. There are also differences in the Doppler spreads measured recently and those

reported by *Angling et al.* [1998]. The recent observations have much smaller spreads; this is particularly marked for the Svalbard-Kiruna path where the maximum spread exceeded 5% of the time is 3.6 Hz compared to 22.2 Hz in the earlier experiment.

[19] The effective multipath spread tends to decrease with frequency for the longer path, while for the shorter path it tends to be lower for the middle frequencies. In most cases, the value is less than 1 ms.

[20] For the purposes of this paper, we have not considered the variations in directional parameters associated with changes in the geomagnetic conditions (i.e., between quiet and disturbed times). Such variations do occur, however the primary purpose of this paper is to present information on directional spread with the aim of using this in the development of engineering simulations of the channel (and to present a methodology of employing these parameters). The geophysical aspect will be considered in a future paper.

4. Channel Modeling

[21] As is apparent from the data presented earlier, HF propagation over high-latitude paths is complex and consequently modeling the channel characteristics is a difficult problem. Large-scale features and their temporal development can be modeled through ray-tracing techniques such as presented by *Zaalov et al.* [2005]. Enhancements to such a model may be made to incorporate Doppler effects and hence the capability to characterize the channel in terms of its scattering function. Such an approach would be computationally time consuming, but is an extension to the work reported by *Zaalov et al.* [2005] which will be addressed in future studies. In order to account for the stochastic signal fluctuations due to the small-scale structure, an approach similar that of *Gherm and Zernov* [1998] could be employed, however the high-latitude ionosphere contains structure on scales ranging from small to extremely large (hundreds of kilometers) making this approach difficult. In view of these difficulties, a parameterized model has been developed with the aim of providing an approximation to the channel scattering characteristics, which include directional effects, suitable for the testing of multichannel processing algorithms (e.g., spatial filtering and direction finding techniques).

4.1. Model Details

[22] Measurements and statistics of the overall angular spreads as reported above are insufficient for defining the channel scattering (including direction) functions. However, it is useful to note the occurrence statistics of particular levels of spreading in applying various channel models. This problem is compounded by the fact that the

propagation environment is very complex and very variable, making a simple parameterization of the channel impossible. For this reason, a significant number of individual soundings have been manually examined and a series of test cases, which are representative of the character of the received signals, defined. These may either be used as they stand, or employed as the basis for further test scenarios.

[23] The diffuse directional characteristics of the channel may be modeled as one or more grids of point sources distributed in both azimuth and elevation, each grid corresponding to a particular time of flight. The separation of the sources in the grid is not particularly critical (a separation of 0.1° has been employed by the authors) but should be chosen so as to be sufficiently small that the individual components would not be resolved by subsequent processing algorithms. An unnecessarily small a spacing results in increased computation times.

[24] Each grid is specified in terms of spreads in azimuth and elevation, with the time varying nature of the diffuse reflections accounted for by angular dependent Doppler shifts separately specified as Doppler spreads in azimuth and elevation. The spatial power distribution is represented as a raised cosine amplitude distribution with the peak at the nominal direction of arrival. Imposition of directionally dependent Doppler shifts is also a way of ensuring that the signals from different directions are incoherent (such incoherence is undoubtedly the case in practice as the individual scatterers are short lived and random in nature).

[25] Each grid is specified by a number of parameters, given below:

  A   azimuth;
  Δ_A azimuthal spread;
  E   elevation;
  Δ_E elevational spread;
  Φ overall Doppler shift;
  $\Delta_{\Phi,A}$ Doppler spread in azimuth direction;
  $\Delta_{\Phi,E}$ Doppler spread in elevation direction;
  δ spacing of the individual components;
  τ time step between samples.

[26] The grid of sources is defined with azimuth values α stepping by δ in the range $A - 0.5\Delta_A$ to $A + 0.5\Delta_A$ and with elevation values ε stepping by δ in the range $E - 0.5\Delta_E$ to $E + 0.5\Delta_E$.

[27] The normalized complex amplitude observed at an antenna with polar coordinates r, θ, with the phase relative to that which would be observed at the origin, from a signal component arriving from an azimuth of α and elevation ε is given by

$$S_{\alpha,\varepsilon,r,\theta} = \exp\left(j\frac{2\pi r \cos(\theta - \alpha)\cos(\varepsilon)}{\lambda}\right). \quad (1)$$

[28] A raised cosine amplitude taper is applied to take the amplitude to zero at the extremes of the grid. This is given by

$$W_{\alpha,\varepsilon} = \sqrt{1 + \cos\left(2\pi\frac{\alpha - A}{\Delta_A}\right)} \cdot \sqrt{1 + \cos\left(2\pi\frac{\varepsilon - E}{\Delta_E}\right)}. \quad (2)$$

[29] It is not physically realistic for all of the components of the grid to start in phase. For this reason the starting phases are randomized by

$$R_{\alpha,\varepsilon} = \exp(j2\pi f_{rand}), \quad (3)$$

where f_{rand} is a random function returning values, with equal probability, in the range 0 to 1. The time varying nature of the signal is modeled by the application of Doppler spreads to the grid in both azimuth and elevation. An overall Doppler shift is also allowed. The phase advance per time step due to the Doppler shifts are given by

$$D_{\alpha,\varepsilon} = \exp(j2\pi\tau\Phi) \cdot \exp\left(j2\pi\tau\Delta_{\Phi,A}\frac{\alpha - A}{\Delta_A}\right)$$
$$\cdot \exp\left(j2\pi\tau\Delta_{\Phi,E}\frac{\varepsilon - E}{\Delta_E}\right). \quad (4)$$

The above equations (1)–(3) may be combined to give the starting signal components within the grid:

$$C_{\alpha,\varepsilon,r,\theta,0} = \frac{S_{\alpha,\varepsilon,r,\theta}W_{\alpha,\varepsilon}R_{\alpha,\varepsilon}}{\sqrt{\sum_{\alpha,\varepsilon}|W_{\alpha,\varepsilon}|^2}}, \quad (5)$$

where the denominator is a normalization term to compensate for the varying number of signal components within each grid.

[30] For each successive time step (numbered as n such that the time t is given by $n\tau$), the new signal complex amplitude components are given by

$$C_{\alpha,\varepsilon,r,\theta,n} = C_{\alpha,\varepsilon,r,\theta,n-1}D_{\alpha,\varepsilon}. \quad (6)$$

and the signal samples at each antenna given by the sum of the components within the grid:

$$X_{r,\theta,n} = \sum_{\alpha,\varepsilon} B_{\alpha,\varepsilon}C_{\alpha,\varepsilon,r,\theta,n}, \quad (7)$$

where $B_{\alpha,\varepsilon}$ represents the directional amplitude sensitivity characteristic (beam pattern) of each receiving antenna.

Table 4. Parameters Associated With Each of the Test Cases[a]

Amplitude	Delay, ms	Φ, Hz	A, deg	Δ_A, deg	$\Delta_{\Phi,A}$, Hz	E, deg	Δ_E, deg	$\Delta_{\Phi,E}$, Hz
			Case A					
1	2.4	0	60	10	1	45	1	1
			Case B					
1	1.6	0	60	5	1	8	5	1
			Case C					
1	2.6	−1	65	50	7	55	1	1
1.5	2.6	0	70	20	4	55	0	0
			Case D					
0.25	3.9	0	−5	0	2	5	15	0
1	4.5	0	−5	0	2	25	10	0
0.25	5.0	0	−5	0	2	25	10	0
			Case E					
1	5.11	20	5	5	8	32	10	8
1	4.9	−15	−15	10	40	25	10	20
			Case F					
1	4.0	2	−5	5	2	8	10	2
1	4.4	0	−10	20	25	28	10	25
1	4.7	0	−10	20	25	28	10	25
			Case G					
1	3.95	0	−5	0	3	12	0	0
1	4.15	0	−5	0	3	25	5	0
2.2	5.15	−1	−5	10	5	32	10	5
2.0	5.4	1	0	10	5	40	5	0
			Case H					
1	4.1	0	−5	0	−4	12	12	4
0.3	4.3	−2	0	10	8	25	15	6
0.2	5.6	0	20	30	5	40	15	0
0.1	5.7	4	−35	20	4	28	5	4
			Case I					
1	2.3	5	30	10	8	33	8	0
0.7	2.6	0	20	10	8	25	10	0
0.5	2.3	−5	82	5	5	40	0	0
0.3	3.1	0	20	10	8	25	10	0
			Case J					
1	1.9	−2	50	25	7	25	15	0
1.8	3.9	0	30	30	30	40	10	0
0.9	4.7	0	20	20	30	40	10	0
0.4	5.7	0	20	20	20	35	10	0
			Case K					
1.6	1.8	0	80	20	6	35	20	6
1	2.1	5	60	20	10	35	20	20
1	2.5	5	60	20	10	35	20	20
1	2.7	5	50	20	10	60	5	20
1	2.1	−5	40	30	10	35	20	20
1	2.8	−5	45	20	10	60	5	10

[a]Cases A, B, C, I, J, and K are based on Kirkenes-Kiruna measurements (great circle bearing 61°). Cases D, E, F, G, and H are based on Svalbard-Kiruna measurements (great circle bearing −5°).

[31] The overall channel dispersion can be modeled as a number of the above grids with appropriate amplitude weighting, one (or more) grids associated with each propagation delay. Since the grids are essentially delta functions in terms of delay, a filter may be applied to give each grid a time delay spread. Additionally, such a filter can merge several grids with different, but closely separated, delays into a single time spread mode. Such a function may, in effect, arise because of the presence of a filter associated with the receiver and it may not be necessary to have two filter functions in the simulation: In the case of the scenarios presented as test cases here, a 2.4 kHz bandwidth was employed approximating that of the receiver bandwidth. The channel simulation is then achieved through the convolution of the data signal with the channel dispersion function defined above. It is important to note that the transmitter and receiver bandwidths are likely to have a significant effect on the signal and that appropriate filtering must therefore be included.

[32] The propagation model may be further complicated by noting that, particularly if wider bandwidths are considered, the propagation delay may also be a function of angle since the off–great circle components will have traveled further than the specularly reflected component.

4.2. Test Cases

[33] A number of test cases have been selected from the examination of a large number of individual soundings. These are representative of the characteristics of the received signals over both the Svalbard-Kiruna and Kirkenes-Kiruna paths. Descriptions of the signal characteristics of these test cases are given below and details of the associated simulation parameters are given in Table 4. An example sounding produced by simulation using the parameters of test case K is presented in Figure 6.

[34] Test case A: This example has a single peak of great circle azimuth, high elevation angle and narrow delay and Doppler spreads.

[35] Test case B: Again a single peak which is narrow in delay and Doppler spreads and on the great circle azimuth. However the elevation angle is about 10° and the delay is smaller.

[36] Test case C: This example has a single peak with narrow delay spread and medium Doppler spread. The elevation angle is consistently high, but the azimuth angle, which varies by 50°, is strongly correlated to the Doppler shift, the northerly azimuths being associated with negative Doppler frequencies, and the easterly azimuths with positive Doppler frequencies. The extreme azimuths are approximately equidistant from the GC azimuth of about 60° east of north.

[37] Test case D: Here, a main great circle peak has narrow spread in both delay and Doppler. Elevation decreases with delay from 30° to 20° over a delay
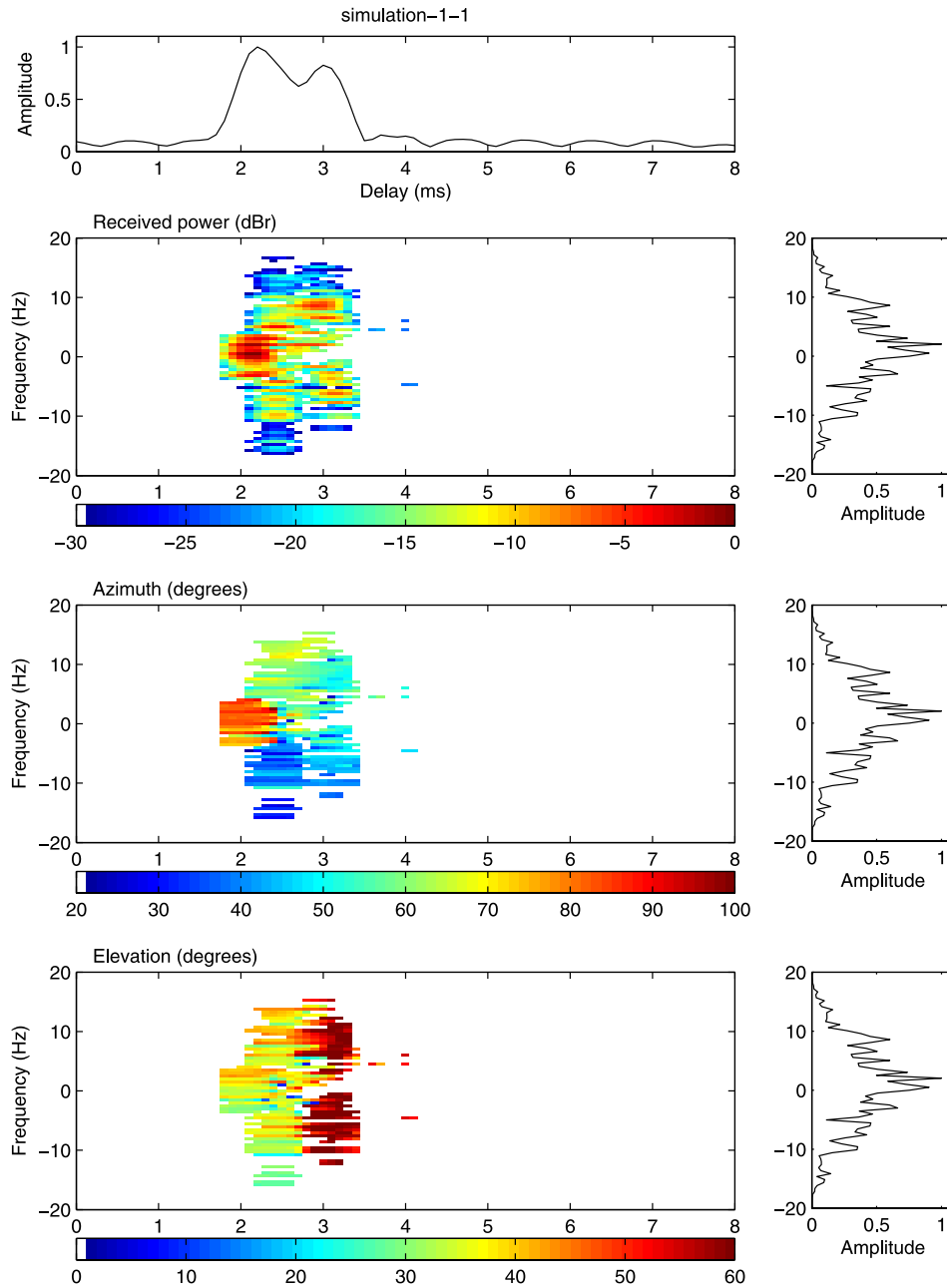
Figure 6. Example sounding produced by simulation using the parameters of test case K. This simulation is broadly reminiscent of the data of Figure 3.

interval of about 1 ms. There is also a small low-elevation angle peak just before the main peak.

[38] Test case E: The main peak has a very broad Doppler spread from around zero to at least −30 Hz. The part of the signal near zero Doppler is from an azimuth about 10° west of north, corresponding to the expected great circle direction, while the low Doppler frequencies are up to 20° west of this, and slightly delayed, giving a peak of medium width in time. This peak has an elevation of 20°–25°. Another peak is seen at the same delay a Doppler width of 10 Hz centered on +20 Hz. It has an azimuth 10° north of GC and an elevation of 30°–35°.

[39] Test case F: A small low-elevation peak of Doppler spread <5 Hz is followed closely by a very broad one (−10 to +10 Hz) of midelevation. Both are close to great circle direction. The peaks overlap to give a delay peak of medium breadth.

[40] Test case G: An initial small peak has an elevation rising from 10° to 25° in 1 ms, and is followed by a larger peak at high elevation. Both are within 10° of the great circle direction. The first peak has a narrow Doppler range, while the second is midrange, with an increase of 5° elevation across its Doppler and delay range.

[41] Test case H: A large peak can be seen distinctly from two simultaneous small peaks at longer delay. The main peak is near GC and of elevation 10° to 25°. The higher-elevation end is slightly later and of lower Doppler shift. The later peaks are high elevation east of GC and midelevation west of GC. The easterly peak has a Doppler frequency similar to the large peak, while the westerly one has a higher Doppler frequency.

[42] Test case I: Here, a peak of medium width in delay and Doppler spread is divisible into two by azimuth. Most of the peak is from a direction to the north of the GC, but a small portion, at the lower end of the delay and Doppler range, comes from the east (GC is at 60° east of north). The elevation is a mixture of medium and high values for both portions with no distinct correlation to delay or Doppler.

[43] Test case J: A small, low-delay GC peak is followed 2 ms later by one which is very broad in delay and Doppler. The latter has a slowly decaying tail that stretches to a very unusual 7 ms delay, though it represented in the model by successive peaks out to about 6 ms. The later peak is mainly from the north, but is nearer GC on its leading edge. The elevation of the first peak is a mixture of middle and low, while that of the second is middle to high.

[44] Test case K: This peak is broad in delay and Doppler, being composed of several overlapping components. Its rather complicated azimuthal structure can, for simplicity, be divided into three parts. The higher Doppler end centers on the GC azimuth (60° east of north), while the lower centers on an azimuth about 40° east of north. However, each varies from these central values by ±10° in patches. Finally there is an area which comes from east of the GC which is confined to medium Doppler frequencies and low delay. The elevation can be split into a first half, which is middle to high, and the later half, which is consistently high.

5. Concluding Remarks

[45] Channel simulation is an important tool in the development of HF communication systems. Single channel simulators (e.g., those based on the *Watterson*

et al. [1970] model) have been around for a number of years and, in general, are appropriate for midlatitude propagation characteristics. Propagation at northerly latitudes is much more complex than that at midlatitudes, particularly so when it is necessary to take into account directional effects (e.g., in direction finding systems, adaptive antenna systems, etc). In order to address this latter problem, measurements of the directional characteristics of signals received over two northerly paths have been made over a prolonged period. On the basis of these measurements, a channel model incorporating directional effects has been developed and a number of test cases that are representative of the complex range of measurements identified. The model is capable of reproducing the nature of the test soundings, and it is therefore suggested that it can be applied in the development and testing of new multichannel processing algorithms.

References

Angling, M. J., and N. C. Davies (1999), An assessment of a new ionospheric channel model driven by measurements of multipath and Doppler spread, paper presented at IEE Colloquium on Frequency Selection and Management Techniques for HF Communications, Inst. of Electr. Eng., London, 1–6 April.

Angling, M. J., P. S. Cannon, N. C. Davies, T. J. Willink, V. Jodalen, and B. Lundborg (1998), Measurements of Doppler and multipath spread on oblique high-latitude HF paths and their use in characterizing data modem performance, *Radio Sci.*, *33*(1), 97–107.

Davies, N. C., and P. S. Cannon (1993), DAMSON—A system to measure multipath dispersion, Doppler spread and Doppler shift on multi-mechanism communications channels, paper presented at AGARD Specialists Meeting on Multiple Mechanism Propagation Paths (MMPPs): Their Characterisation and Influence on System Design, Advis. Group for Aerosp. Res. and Dev., Rotterdam, Netherlands.

Featherstone, W., H. J. Strangeways, M. A. Zatman, and H. Mewes (1997), A novel method to improve the performance of Capon's minimum variance estimator, *Proceedings of the IEE Tenth International Conference on Antennas and Propagation*, IEE Conf. Publ., *436*, 1.322–1.325.

Gherm, V. E., and N. N. Zernov (1998), Scattering function of the fluctuating ionosphere in the HF band, *Radio Sci.*, *33*(4), 1019–1034.

Gherm, V. E., N. N. Zernov, and H. J. Strangeways (2005), HF propagation in a wideband ionospheric fluctuating reflection channel: Physically based software simulator of the channel, *Radio Sci.*, *40*, RS1001, doi:10.1029/2004RS003093.

International Telecommunication Union (2000), Recommendation ITU-R F.1487, Testing of HF modems with bandwidths of up to about 12 kHz using ionospheric channel simulators, Geneva, Switzerland.

Jenkins, R. W. (1994), A simulation study of HF direction finding in the presence of *F*-region scattering and sporadic-*E*, *CRC Tech. Note 93-004*, Commun. Res. Cent. Ottawa.

Jodalen, V., T. Bergsvik, P. S. Cannon, and P. C. Arthur (2001), Performance of HF modems on high-latitude paths using multiple frequencies, *Radio Sci.*, *36*(6), 1687–1698.

Read, W. J. L. (1999), Advanced DF algorithms for high latitude operation, paper presented at Third Symposium on Radiolocation and Direction Finding, Southwest Res. Inst., San Antonio, Tex.

Warrington, E. M. (1998), Observations of the directional characteristics of ionospherically propagated HF radio channel sounding signals over two high latitude paths, *IEE Proc. Microwaves Antennas Propag.*, *145*(5), 379–385.

Warrington, E. M., C. A. Jackson, and B. Lundborg (2000a), Directional diversity of HF signals received over high latitude paths and the possibility of improved data throughput by means of spatial filtering, *IEE Proc. Microwaves Antennas Propag.*, *147*(6), 487–494.

Warrington, E. M., A. J. Stocker, and C. Rizzo (2000b), Behaviour of superresolution direction finding algorithms for HF signals propagating through the high latitude ionosphere, *IEE Proc. Microwaves Antennas Propag.*, *147*(6), 469–478.

Watterson, C. C., J. R. Juroshek, and W. D. Bensema (1970), Experimental confirmation of an HF channel model, *IEEE Trans. Commun. Technol.*, *18*, 792–803.

Zaalov, N. Y., E. M. Warrington, and A. J. Stocker (2003), Simulation of off-great circle HF propagation effects due to the presence of patches and arcs of enhanced electron density within the polar cap ionosphere, *Radio Sci.*, *38*(3), 1052, doi:10.1029/2002RS002798.

Zaalov, N. Y., E. M. Warrington, and A. J. Stocker (2005), A ray-tracing model to account for off-great circle HF propagation over northerly paths, *Radio Sci.*, *40*, RS4006, doi:10.1029/2004RS003183.

—————

D. R. Siddle, A. J. Stocker, and E. M. Warrington, Department of Engineering, University of Leicester, Leicester LE1 7RH, UK. (emw@le.ac.uk)